A STUDY ON THE STRESS CONCENTRATION FACTOR INDUCED IN DOUBLE COUNTERSUNK HOLES DUE TO UNIAXIAL TENSION

MOHAMMAD A. GHARAIBEH
Mechanical Engineering Department
Hashemite University
Zarqa, 13133, JORDAN
E-mails: mohammada_fa@hu.edu.jo

Finite element and response surface methods were utilized to investigate the stress concentration factor induced in isotropic rectangular plates with two identical countersunk rivet holes due to uniaxial tension. In this investigation, the finite element model was constructed using ANSYS software and used to produce stress concentration factor (SCF) data. Additionally, the response surface method (RSM) was implemented to characterize the influence of the problem geometric parameters on the SCF. Besides, RSM combined with least squares regression methods were employed to formulate a simple and effective equation to mathematically compute the stress concentration factor (K_t) value. This equation was consequently verified with finite element analysis (FEA) results. Lastly, an optimum plate and holes configuration that minimizes the SCF was suggested and hence recommended.

Key words: double countersunk holes, stress concentration factor, finite element method, response surface method, and uniaxial tension.

1. Introduction

Riveting is a common and widely used method of joining mechanical and structural components. Countersunk holes are common footprint resulting from rivet joints. The presence of such geometric irregularities acts as stress risers throughout the thickness of the joined structure, i.e. elastic plates, which further complicates the stress distributions resulting in stress concentration regions. Stress concentrations are often described using the measures of stress concentration factors (SCF). The stress concentration factor (K_t) is mathematically defined as the ratio between the maximum stress (σ_{max}) and the average or nominal stress value (σ_{nom}), as

$$K_t = \frac{\sigma_{max}}{\sigma_{nom}}. \tag{1.1}$$

In real-life engineering applications, rivets are generally drilled in multiple and in non-similar configurations which further adds to the complexity of the stress concentration analysis in the neighborhood of the countersunk holes. In literature data, stress concentration factors have been widely studied and numerous data on the SCF induced in different stress risers under various loading conditions are available [1, 2]. A common and simple stress riser problem is the centrally-drilled circular hole in plates subjected to uniaxial loading. For this problem, Shivakumar *et al*. [3, 4] used the finite element analysis (FEA) to investigate the SCF in central circular holes in thick and thin plates with uniaxial tension. The results showed that the region of stress concentration is located near the hole edge normal to the loading direction for both thin and thick plate systems. Several experimental, numerical and analytical investigations are reported in literature for the area of the SCF in circular holes under different loading environments [5-9].

For the investigation of the SCF in countersunk holes, Whaley [10] and Cheng [11] performed experimental analysis to study the stress distributions at the top and bottom as well as in the interior of the countersunk holes showing that the local maximum stress occurs at the sinking edge of the hole. Bhargava *et al*. [12] and Shivakumar *et al*. [13, 14] performed thorough three-dimensional FEA studies on the SCF in uniaxially loaded isotropic and orthotropic plates with central countersunk holes. Their simulation results showed that the stress concentration is commonly located at the sinking edge of the hole and they further used the numerical data to formulate an empirical formulas to mathematically compute K_t in countersunk holes based on the geometry of the hole. Later, Gharaibeh *et al*. [15] and Darwish *et al*. [16, 17] provided improved formulas for the SCF in countersunk holes in isotropic and orthotropic plates subjected to uniaxial tensile loadings. Hayajneh *et al*. [18] and Bhargava *et al*. [19] investigated the strain concentration factor (SeCF) in countersunk holes under uniaxial tension. Both showed that the SeCF, similar to the SCF, occurs at the sinking edge of the hole. Additionally, they found that the SeCF is mathematically related to the SCF. Also, Bhargava *et al*. [19] provided an empirical formula to compute SeCF in countersunk holes in an isotropic plate subjected to remote uniaxial tensile loading. For the plate with double countersunk holes, Darwish *et al*. [20] employed FEA simulations to produce a parametric study on the effect of the plate and the holes geometries on the SCF in uniaxially-loaded plate with two identical countersunk holes.

The present paper aims to utilize the finite element method (FEM) and response surface methods (RSM) to study and investigate the stress concentration factor induced in a plate with two identical countersunk holes subjected to uniaxial tension that is perpendicular to the holes line. In this investigation, a simple and precise second order equation to calculate K_t in the double-holes configuration is formulated and validated accordingly. Finally, an optimal geometric design of the holes and the plate is recommended and hence verified.

2. Configuration and material

The geometric details of a plate with two identical countersunk holes are presented in Fig.1. This figure defines the geometric parameters of the present problem as: the plate length (*2L*), width (*2w*) and thickness (*t*). Note that the plate consists of two parts: the straight shank thickness (*b*) and the sinking depth (C_s), such that $(t = b + C_s)$. Also, the straight shank radius is (*r*) and the countersink angle is (θ_c) and the separating distance between the centers of the holes is $(2w_h)$.
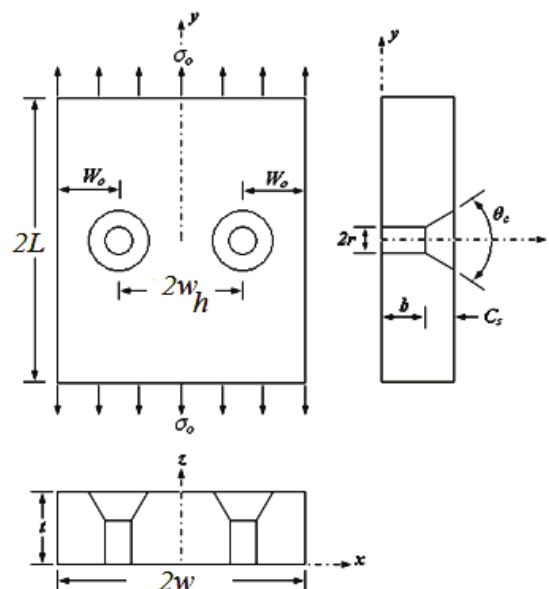

Fig.1. Configuration of the double countersunk hole.

In the current analysis, homogenous isotropic and linear elastic properties of the plate system with a modulus of elasticity of ($E = 70GPa$) and Poisson's ratio of ($\nu = 0.3$) were considered. For such material system, the stress and strain concentration values are independent of E [21].

Utilizing finite element (FE) and response surface methods, a comprehensive analysis is performed to investigate the K_t values in the double countersunk holes at different countersink angles (θ_c), thickness to radius ratio (t/r), countersink depth to plate thickness ratio (C_s/t) and radius to width ratio (r/w) as well as normalized separating distance ($\lambda = w_h/w$). To exclude the influence of the plate length on K_t, the plate length to the radius ratio is kept constant at ($L/r = 15$) throughout the analysis. Using the FEA data and using nonlinear regression, an empirical formula for K_t is developed and hence validated.

3. Finite element modeling

ANSYS Mechanical version 19.0 was used to build the finite element model, define geometric and material parameters and to apply loading and boundary conditions of the present problem and to execute the analysis. Per the symmetry of the problem, only one symmetric half model was considered. In this half model, symmetric boundary conditions were specified by setting the displacement in the *y* - direction to zero $\left(u_y = 0\right)$ on the *y=0* plane of symmetry. Additionally, two nodes located at $x = \pm w, y = l$ and *z=0* were restrained in the *z* - direction $\left(u_z = 0\right)$ to prevent the out-of-plane motion. For load application, a unity remote stress $\left(\sigma_o = 1\right)$ was imposed on *y=l* surface, as depicted in Fig.2.
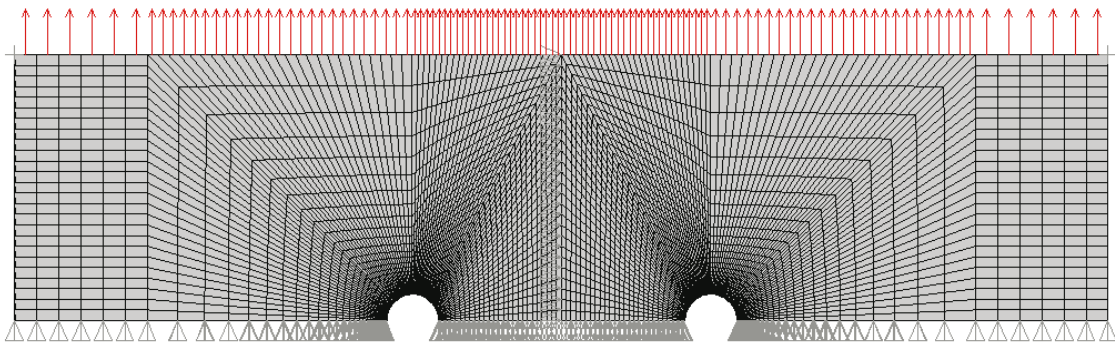

Fig.2. Loading and boundary conditions applied on the symmetric half model.

For the FEA mesh design, only three dimensional hexahedron elements, defined as SOLID185 in ANSYS, were adopted to generate the mapped FEA mesh. Additionally, care was taken to have a finer mesh near the hole and a relatively coarser mesh elsewhere, as shown in the figure. This was done to ensure best stress solution accuracy at the area of interest with minimum FE model solution time. Furthermore, the finite element mesh adequacy was tested in order to ensure best strain results accuracy with minimum solution time. This model contained 95,400 elements and 105,222 nodes.
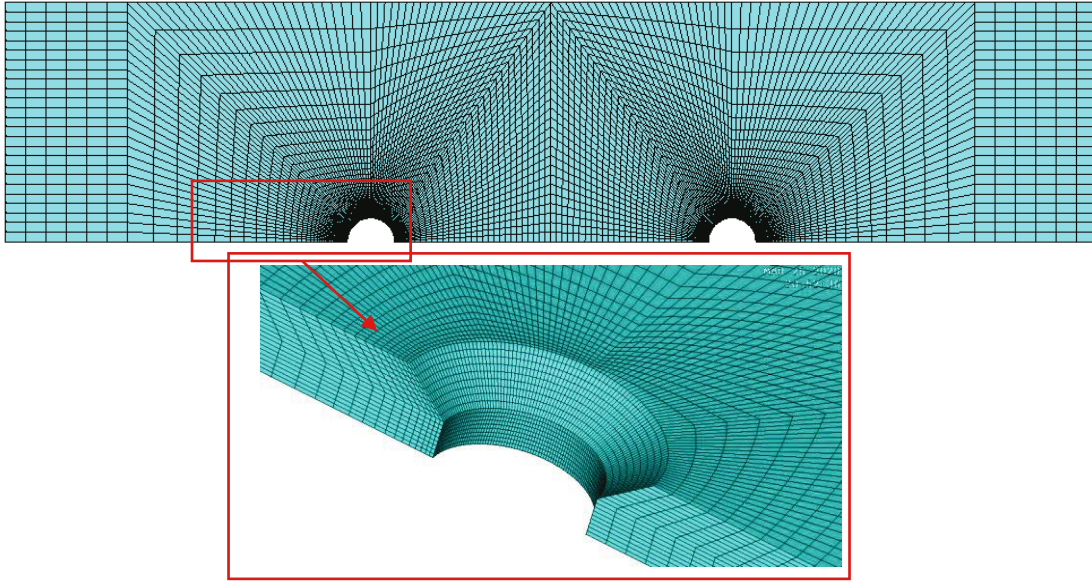
Fig.3. The final FEA mesh configuration.

4. Stress concentration factor analysis using RSM

The response surface methodology (RSM) is often defined as an aggregation of mathematical and statistical expressions that are helpful for the analysis of engineering problems in which a particular response (output) of interest is generally a function of several independent variables (inputs) and the main goal is optimize, i.e. maximize or minimize, this particular response. Generally, the RSM is used to fit a second order response surface. Additionally, the RSM characterizes the main and the interaction effects of the independent input variables on the output response based on a minimum number of experimental and/or numerical runs. Here, the RSM was utilized to investigate and optimize, i.e. minimize, the stress concentration factor in a plate with two identical countersunk holes under uniaxial tension.

In the present analysis, MINITAB Release 19.1 was used to implement the RSM design and to execute the optimization process. As summarized in Table 1, five independent variables, including the radius to width (r/w) ratio, thickness to radius (t/r) ratio, countersinking depth to thickness (C_s/t) ratio, countersink angle (θ_c) and normalized separating distance (λ) were spread over three consecutive levels: low level (-1), middle level (0) and high level (+1). A central composite design (CCD) with half-factorial design $\left(1/2 \times 2^n\right)$, axial points ($2n$) and central points, where n is the number of independent input variables ($n=5$), was conducted. In this CCD analysis, 32 FEA runs were necessary per the general equation $\left(1/2 \times 2^n + 2n + 6 = 32\right)$ in which the FEA runs were improved by 6 replicate runs at the central design point, as recommended by MINITAB. In order to obtain and fit a second order surface equation of (K_t), the following expression was considered

$$K_t = a_o + \sum_{i=1}^{n} a_i X_i + \sum_{i \leq j} \sum a_{ij} X_i X_j + \sum_{i=1}^{n} a_{ii} X_{ii}^2 + e \tag{4.1}$$

where X_i and X_j are the independent variables; a_o is the constant coefficient; a_i, a_{ii} and a_{ij} are the interaction coefficients of the linear, quadratic and second order terms, respectively; and e is the random relative error.

Table 1. The CCD of the five independent variables.

Independent Variables	RSM Levels		
	Low level (-1)	Middle level (0)	High level (+1)
Radius to width ratio (r/w)	*0.1*	*0.2*	*0.3*
Thickness to radius ratio (t/r)	*1*	*2*	*3*
Countersink depth to thickness ration (C_s/t)	*0.1*	*0.3*	*0.5*
Countersink angle (θ_c)	*80°*	*100°*	*120°*
Normalized separating distance (λ)	*0.25*	*0.5*	*0.75*

5. Results and discussions

5.1. Central composite design

As mentioned earlier, the main objective of this investigation was to analyze and optimize the SCF in double countersunk holes configuration. The minimization of the SCF is generally favorable for safe structural designs. The simulation results of the 32 CCD runs performed in this analysis are listed in Appendix **1**. As shown in this appendix, the highest value ($K_t = 6.013$) is achieved in run #32 were ($r/w = 0.3$, $t/r = 3$, $C_s/t = 0.5$, $\theta_c = 120°$ and $\lambda = 0.75$). Hence, these geometric parameters of the double countersunk holes problem are highly not recommended.

5.2. Regression and residuals analysis

In this work, the first proposed form of the (K_t) equation included all the previously described independent variables, as

$$K_t = a_0 + a_1\left(\frac{r}{w}\right) + a_2\left(\frac{t}{r}\right) + a_3\left(\frac{C_s}{t}\right) + a_4\theta_c + a_5\lambda + a_{11}\left(\frac{r}{w}\right)^2 + a_{22}\left(\frac{t}{r}\right)^2 +$$

$$+ a_{33}\left(\frac{C_s}{t}\right)^2 + a_{44}(\theta_c)^2 + a_{55}\lambda^2 + a_{12}\left(\frac{r}{w}\right)\left(\frac{t}{r}\right) + a_{13}\left(\frac{r}{w}\right)\left(\frac{C_s}{t}\right) + a_{14}\left(\frac{r}{w}\right)\theta_c + \tag{5.1}$$

$$+ a_{15}\left(\frac{r}{w}\right)\lambda + a_{23}\left(\frac{t}{r}\right)\left(\frac{C_s}{t}\right) + a_{24}\left(\frac{t}{r}\right)\theta_c + a_{25}\left(\frac{t}{r}\right)\lambda + a_{34}\left(\frac{C_s}{t}\right)\theta_c + a_{35}\left(\frac{C_s}{t}\right)\lambda + a_{45}\theta_c\lambda,$$

which included 21 equation terms. However, to reduce model complexity without affecting model accuracy, model reduction was necessary and achieved by eliminating the insignificant terms. Thus, the final form of K_t equation is given by

$$K_t = 6.634 - 6.88\left(\frac{r}{w}\right) + 0.164\left(\frac{t}{r}\right) - 3.68\left(\frac{C_s}{t}\right) - 0.029\theta_c +$$

$$-5.33\lambda + 3.07\lambda^2 + 11.21\left(\frac{r}{w}\right)\left(\frac{C_s}{t}\right) - 0.07\left(\frac{r}{w}\right)\theta_c + 0.041\left(\frac{C_s}{t}\right)\theta_c + 0.018\theta_c\lambda. \tag{5.2}$$

It is important to mention here that the above equation has only 11 terms with achieving a coefficient of determination value of $R^2 = 95.83\%$ which strongly indicates high accuracy of the reduced model of Eq.(5.2). A comparison between Eq.(5.2) calculations and FEA data is included in Appendix 1. From this comparison, it can be concluded that, based on the $\%Error = \dfrac{FEA - Eq.(4)}{FEA} * 100\%$ values, the fitted formula of Eq.(5.2) can accurately predict the K_t value. Additionally, in order to have a valid RSM model, it

is required for the residuals (errors between FEA and predicted results) to be normally distributed, uncorrelated to each other and have a constant variance. To prove this, Fig.4 shows the graphs for the residuals of Eq.(5.2). Residual graphs prove that the residuals are normally distributed (Fig.4a), uncorrelated to each other (Fig.4b) and have constant variance (Fig.4c). This means that the assumptions of the least squares method that was used to fit Eq.(5.2) are fully satisfied.
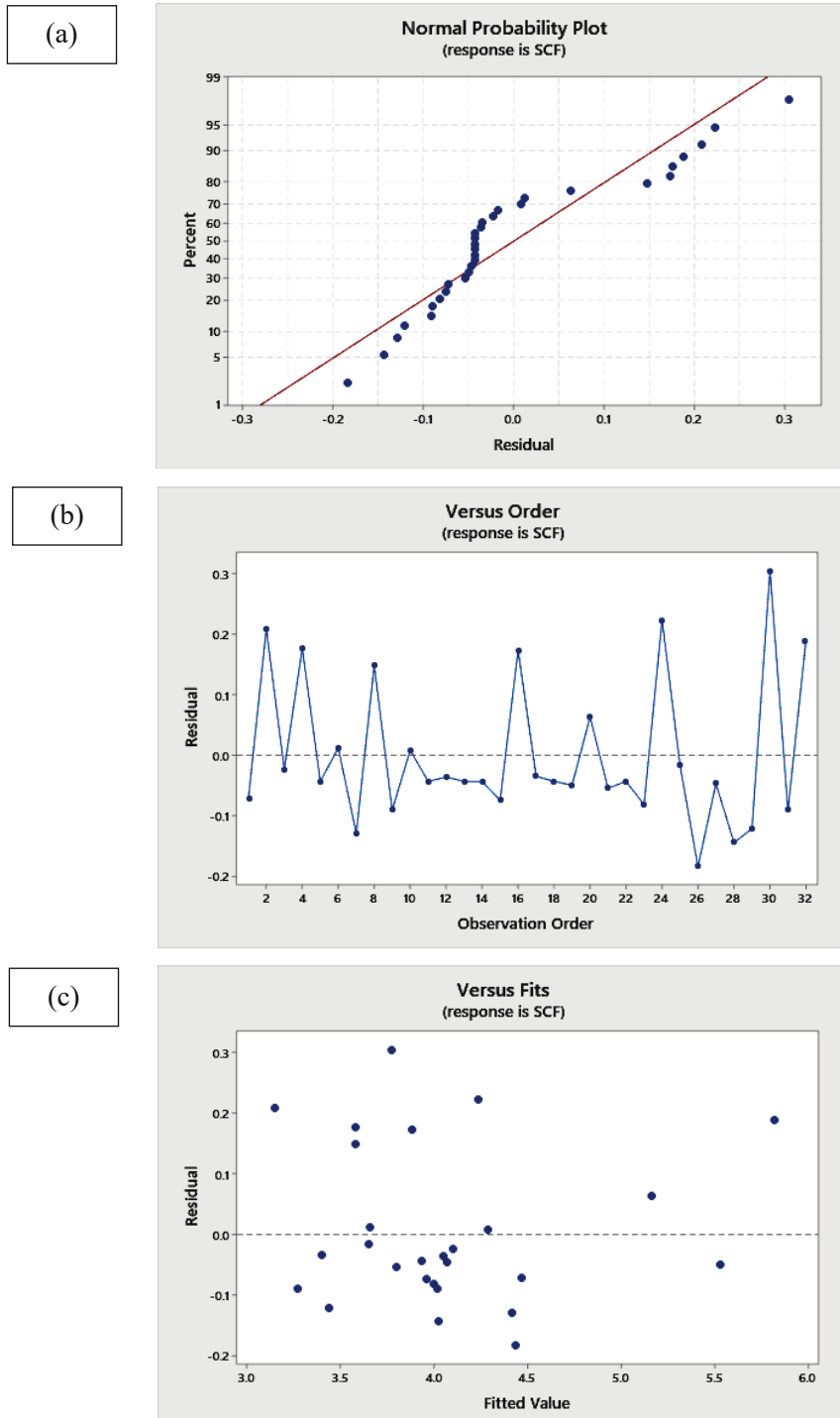

Fig.4. Residuals plots for K_t response.

5.3. Main effects of the geometric parameters

Fig.**5** depicts the effect of (r/w, t/r, C_s/t, θ_c and λ) geometric factors on the K_t value. It can be seen from this figure that the K_t response increases as r/w, t/r, C_s/t and θ_c increase. Additionally, the effects of r/w and C_s/t are much more significant than the other factors as appears from the higher slopes in the r/w and C_s/t subplots. For the effect of the normalized separating distance (λ), it appears that at small values $\lambda=0.25$ the value of K_t is the highest while for $\lambda=0.5$ the value of K_t is the lowest. However, for $\lambda=0.75$ the K_t value is slightly higher than that of $\lambda=0.5$ but much lower than that of $\lambda=0.25$.
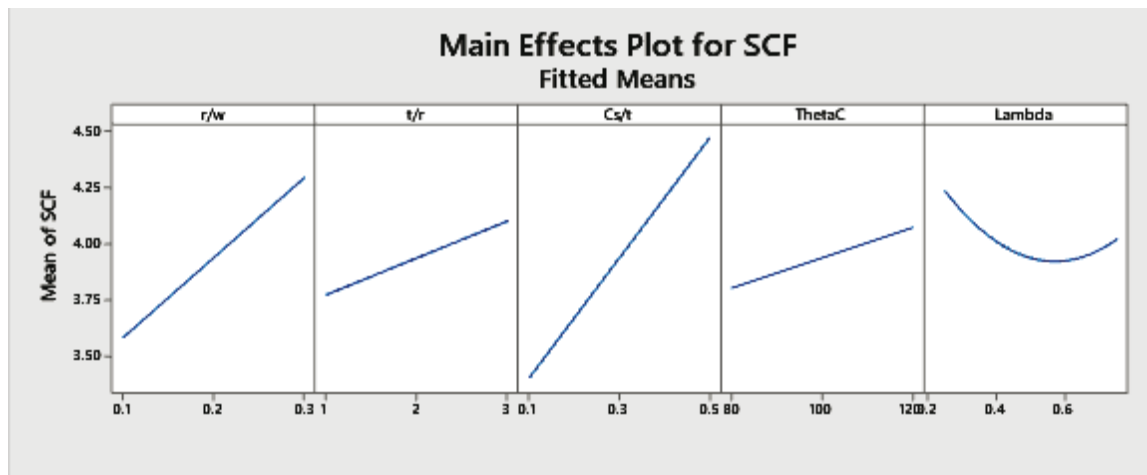

Fig.5. Main effects of the nondimensional geometric parameters on the K_t value.

At this stage of the RSM analysis, it is very convenient to obtain the non-dimensional geometric parameters of the plate and the double countersunk holes configuration that optimize (minimize) the SCF value. This is mathematically achieved by deriving Eq.(5.2) with respect to each independent variable and by equating the resultant equations to zero. Thus, five equations are achieved. By solving these equations simultaneously the optimal design is reached as ($r/w=0.1, t/r=1, C\_s/t=0.1$, $\theta_c=80°$ and $\lambda=0.5$) and the resultant minimum SCF value is $K_t=3.352$. The K_t results of this optimal configuration are compared to FEA findings as listed in Table 2. This comparison shows that the optimal results of FEA and Eq.(5.2) both are within the specified confidence interval ($CI=95\%$) bounds, which additionally confirms the adequacy of Eq.(5.2) prediction model. The stress contour plot from FEA simulations of this optimal system is presented in
Fig.**6**. This plot shows that the nominal stress value in the plate is $\sigma_{nom}=1Pa$ and the maximus stress, located at the sinking edge of the hole, is $\sigma_{max}=3.202\,Pa$. Using Eq.(1), it can be easily calculated that $K_t=3.202$.

Table 2. K_t Optimization results.

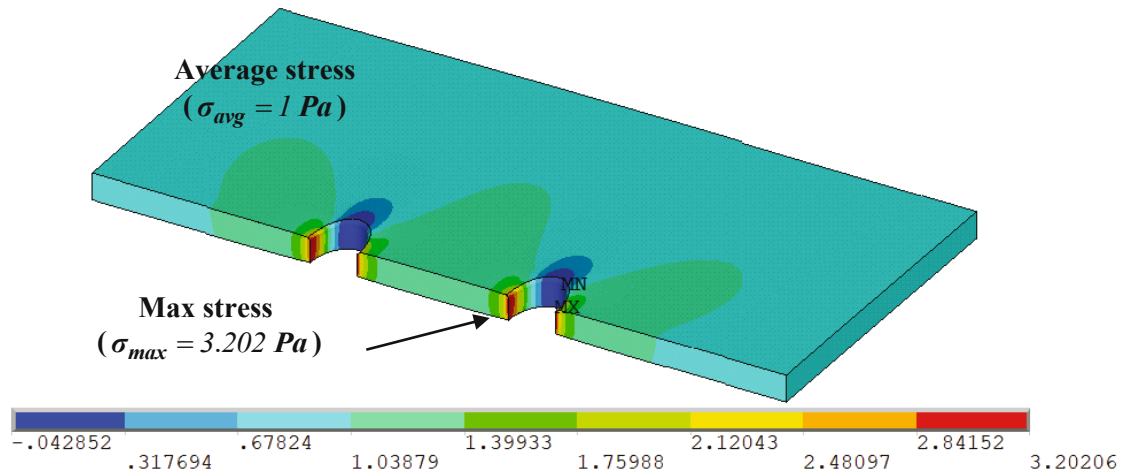|	RSM Model Results			FEA
	Predictions	95% CI low	95% CI high	
K_t	*3.352*	*2.95025*	*3.45328*	*3.202*

Fig.6. FEA results for stress concentration value of the optimal design.

In the summary of this discussion, the RSM results and data presented in this paper are reasonably accurate and able to predict precisely the stress concentration factor value in a uniaxially loaded isotropic rectangular plate with double countersunk rivet holes.

Conclusions

This present paper introduced a study on the stress concentration factor induced in a plate with two identical countersunk holes under uniaxial tension using finite element and response surface methods. An extensive analysis on the influence of the five nondimensional geometric parameters (r/w, t/r, C_s/t, θ_c and λ) on the stress concentration factor value was conducted. By using the means of response surface and ordinary least squares methods, an efficient and precise second order equation of K_t was achieved and hence validated with finite element analysis data. The findings presented in this paper recommend the design of thin plates with two well-separated countersunk holes having small countersink angles and depth as well as small radii to minimize the stress concentration induced due uniaxial tensile loading conditions.

Nomenclature

b − straight shank thickness
C_s − countersink depth
E, ν − modulus of elasticity and Poisson's ratio
FEA − finite element analysis
K_t − stress concentration factor
L − plate half-length
r − straight shank radius
RSM − response surface methodology
SCF − stress concentration factor
SeCF − strain concentration factor
t − plate thickness
w − plate half-width
w_h − half the separating distance between the centers of the countersunk holes
x, y, z − Cartesian coordinate system
θ_c − countersink angle
λ − normalized separating distance between the countersunk holes

Appendix 1. Central composite design results.

Run #	Independent Variables					K_t Response		%Error
	r/w	*t/r*	*C$_s$/t*	θ_C	λ	**FEA**	**RSM Eq.(5.2)**	
1	*0.2*	*2*	*0.5*	*100*	*0.5*	*4.393*	*4.465*	*-1.65*
2	*0.1*	*1*	*0.1*	*120*	*0.25*	*3.352*	*3.143*	*6.23*
3	*0.2*	*3*	*0.3*	*100*	*0.5*	*4.074*	*4.097*	*-0.57*
4	*0.1*	*2*	*0.3*	*100*	*0.5*	*3.753*	*3.576*	*4.71*
5	*0.2*	*2*	*0.3*	*100*	*0.5*	*3.89*	*3.933*	*-1.11*
6	*0.3*	*1*	*0.1*	*120*	*0.75*	*3.667*	*3.655*	*0.33*
7	*0.1*	*3*	*0.5*	*120*	*0.25*	*4.287*	*4.416*	*-3.01*
8	*0.3*	*3*	*0.1*	*80*	*0.75*	*3.725*	*3.576*	*3.99*
9	*0.2*	*2*	*0.3*	*100*	*0.75*	*3.925*	*4.015*	*-2.31*
10	*0.3*	*2*	*0.3*	*100*	*0.5*	*4.298*	*4.289*	*0.19*
11	*0.2*	*2*	*0.3*	*100*	*0.5*	*3.89*	*3.933*	*-1.11*
12	*0.1*	*1*	*0.5*	*120*	*0.75*	*4.015*	*4.050*	*-0.89*
1	*0.2*	*2*	*0.3*	*100*	*0.5*	*3.89*	*3.933*	*-1.11*
14	*0.2*	*2*	*0.3*	*100*	*0.5*	*3.89*	*3.933*	*-1.11*
15	*0.1*	*1*	*0.5*	*80*	*0.25*	*3.881*	*3.955*	*-1.92*
16	*0.1*	*3*	*0.5*	*80*	*0.75*	*4.057*	*3.883*	*4.28*
17	*0.2*	*2*	*0.1*	*100*	*0.5*	*3.366*	*3.401*	*-1.03*
18	*0.2*	*2*	*0.3*	*100*	*0.5*	*3.89*	*3.933*	*-1.11*
19	*0.3*	*1*	*0.5*	*120*	*0.25*	*5.483*	*5.532*	*-0.90*
20	*0.3*	*3*	*0.5*	*80*	*0.25*	*5.226*	*5.162*	*1.21*
21	*0.2*	*2*	*0.3*	*80*	*0.5*	*3.744*	*3.798*	*-1.45*
22	*0.2*	*2*	*0.3*	*100*	*0.5*	*3.89*	*3.933*	*-1.11*
23	*0.1*	*3*	*0.1*	*80*	*0.25*	*3.914*	*3.995*	*-2.08*
24	*0.2*	*2*	*0.3*	*100*	*0.25*	*4.458*	*4.234*	*5.02*
25	*0.3*	*1*	*0.1*	*80*	*0.25*	*3.632*	*3.648*	*-0.46*
26	*0.3*	*1*	*0.5*	*80*	*0.75*	*4.249*	*4.433*	*-4.33*
27	*0.2*	*2*	*0.3*	*120*	*0.5*	*4.021*	*4.067*	*-1.16*
28	*0.3*	*3*	*0.1*	*120*	*0.25*	*3.876*	*4.020*	*-3.72*
29	*0.1*	*3*	*0.1*	*120*	*0.75*	*3.314*	*3.435*	*-3.66*
30	*0.2*	*1*	*0.3*	*100*	*0.5*	*4.074*	*3.768*	*7.49*
31	*0.1*	*1*	*0.1*	*80*	*0.75*	*3.175*	*3.265*	*-2.86*
32	*0.3*	*3*	*0.5*	*120*	*0.75*	*6.013*	*5.824*	*3.14*

References

[1] Pilkey W.D. and Pilkey D.F. (2008): *Peterson's stress concentration factors*. − John Wiley and Sons.

[2] Savin G.N. (1961): *Stress concentration around holes*. − Pergamon.

[3]   Shivakumar K.N. and Newman Jr. J.C. (1992): *Stress concentrations for straight-shank and countersunk holes in plates subjected to tension, bending, and pin loading*. NASA Technical Paper 3192.

[4]   Shivakuma K.N. and Newman J.C. (1995): *Stress concentration equations for straight-shank and countersunk holes in plates*. − Transactions-American Society of Mechanical Engineers Journal of Applied Mechanics, vol.62, pp.248-248.

[5]   Chaudhuri J., Kalman Z.H., Weng G.J. and Weissmann S. (1982): *Determination of the strain concentration factors around holes and inclusions in crystals by X-ray topography*. − Journal of Applied Crystallography, vol.15, No., pp.423-429.

[6]   Pandita S.D., Nishiyabu K. and Verpoest I. (2003): *Strain concentrations in woven fabric composites with holes*. − Composite Structures, vol.59, No.3, pp.361-368.

[7]   Yang Z., Kim C.B., Cho C. and Beom H.G. (2008): *The concentration of stress and strain in finite thickness elastic plate containing a circular hole*. − International Journal of Solids and Structures, vol.45, No.3-4, pp.713-731.

[8]   Ray-Chaudhuri S. and Chawla K. (2018): *Stress and strain concentration factors in orthotropic composites with hole under uniaxial tension*. − Curved and Layered Structures, vol.5, No.1, pp.213-231.

[9]   Berto F., Lazzarin P. and Wang C.H. (2004): *Three-dimensional linear elastic distributions of stress and strain energy density ahead of V-shaped notches in plates of arbitrary thickness*. International Journal of Fracture, vol.127, No.3,pp.265-282.

[10] Whaley R.E. (1965): *Stress-concentration factors for countersunk holes*. − Experimental Mechanics, vol.5, No.8, pp.257-261.

[11] Cheng Y.F. (1978): *Stress-concentration factors for a countersunk hole in a flat bar in tension and transverse bending*.

[12] Bhargava A. and Shivakumar K.N. (2007): *Three-dimensional tensile stress concentration in countersunk rivet holes*. The Aeronautical Journal, vol.111, No.1126,pp.777-786.

[13] Shivakumar K.N., Bhargava A. and Hamoush S. (2007): *A general equation for stress concentration in countersunk holes*. − CMC-TECH SCIENCE PRESS, vol.6, No.2, 71.

[14] Shivakumar K.N., Bhargava A. and Newman J.C. (2007): *A tensile stress concentration equation for countersunk holes*. − Journal of Aircraft, vol.44, No.1,pp.194-200.

[15] Gharaibeh M.A., Tlilan H. and Gharaibeh B.M. (2019): *Stress concentration factor analysis of countersunk holes using finite element analysis and response surface methodology*. − Australian Journal of Mechanical Engineering, vol.1-9.

[16] Darwish F., Gharaibeh M. and Tashtoush G.A. (2012): *Modified equation for the stress concentration factor in countersunk holes*.− European Journal of Mechanics-A/Solids, vol.36, pp.94-103.

[17] Darwish F., Tashtoush G. and Gharaibeh M. (2013): *Stress concentration analysis for countersunk rivet holes in orthotropic plates*. − European Journal of Mechanics-A/Solids, vol.37, pp.69-78.

[18] Hayajneh M., Darwish F.H. and Alshyyab A. (2014): *A modelling strategy and strain concentration analysis for a countersunk hole in an orthotropic plate*. − International Journal of Design Engineering, vol.5, No.3, pp.175-192.

[19] Bhargava A. and Shivakumar K.N. (2008): *A three-dimensional strain concentration equation for countersunk holes*. − The Journal of Strain Analysis for Engineering Design, vol.43, No.2, pp.75-85.

[20] Darwish F., Al-Nasser L. and Al-Araidah O. (2012):*Tensile stress concentration in plates with double countersunk rivet holes.* − International Journal of Design Engineering, vol.5, No.2, pp.158-173.

[21] Timoshenko S.P. and Goodier J.N. (1970): *Mathematical theory of elasticity*. − 3rd edition.